ACS Chemical Neuroscience

pubs.acs.org/chemneuro Research Article

Depression of Pyroptosis by Inhibiting Caspase-1 Activation Improves Neurological Outcomes of Kernicterus Model Rats

Siyu Li, Hongmei Huang, Qian Wei, Chunmei He, Jie Feng, Yao Wang, Mengwen Li, Qiannan Zhang, Xuhua Xia, and Ziyu Hua*

Cite This: *ACS Chem. Neurosci.* 2021, 12, 2929–2939

Read Online

ACCESS | Metrics & More | Article Recommendations

ABSTRACT: Kernicterus is a severe complication of extreme neonatal hyperbilirubinemia. Prolonged exposure to high-level unconjugated bilirubin (UCB) directly damages brain tissue. Neuroinflammation is believed to contribute to UCB-induced neurotoxicity. Pyroptosis has been as a highly inflammatory form of programmed cell death. Therefore, this study aimed to explore whether pyroptosis was involved in the pathogenesis of UCB neurotoxicity in kernicterus model rats. VX-765, a specific inhibitor of caspase-1, was intraperitoneally administered to the model rats to observe its effects on the short-term and long-term outcomes of the model animals at the molecular, cellular, morphological, and behavioral levels. The results indicated that UCB significantly induced the activation of caspase-1 and gasdermin D(GSDMD), and VX-765 inhibited caspase-1-GSDMD pathway. Compared with those of the UCB group and the vehicle+UCB group, VX-765-treated rats released lower levels of IL-1β and IL-18. Furthermore, H&E and TUNEL staining showed that nerve cells in the VX-765-treated group were better preserved and had less DNA fragmentation. Most importantly, VX-765 improved both the short-term and long-term neurological functions of kernicterus model rats. This study demonstrated that pyroptosis was involved in the pathogenesis of kernicterus through caspase-1 activation, which could be inhibited by VX-765, exerting a neuroprotective effect in kernicterus model rats.

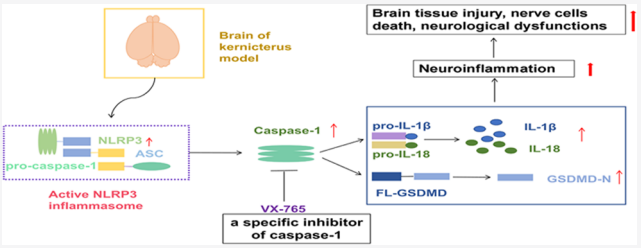

KEYWORDS: *Unconjugated bilirubin, caspase-1, VX-765, neurological outcomes, rats*

INTRODUCTION

Neonatal hyperbilirubinemia is a common condition that is usually considered benign. However, there still remains a high incidence of severe cases despite effective phototherapy and exchange transfusion, especially when the condition is accompanied by other concomitant causes. Prolonged exposure to high-level unconjugated bilirubin (UCB) directly damages brain tissue, leading to a set of bilirubin-induced neurological dysfunctions and eventually to kernicterus, which can be lethal.[1,2]

Recently, abundant studies have been carried out *in vitro* and *in vivo* to explore the potential mechanisms of UCB neurotoxicity, such as endoplasmic reticulum and oxidative stress, neurodegeneration, and neuroinflammation, which are believed to be key contributors to UCB-induced neurotoxicity.[3,4] More importantly, the studies reported that administration of minocycline had a remarkable anti-inflammatory effects in a rat kernicterus model.[4−6] However, due to the effects on developing bones and teeth, minocycline is clinically prohibited for newborns. Thus, we aim to further explore whether there are new potential therapeutic pathways that could be used to rescue UCB-induced neuroinflammation in a rat kernicterus model.

Pyroptosis is a highly inflammatory form of programmed cell death caused by the activation of inflammatory caspase proteins, such as caspase-1 and caspase-11. Caspase-1 is activated by the canonical inflammasomes, and when activated, it cleaves gasdermin D(GSDMD) to generate an N-terminal cleavage product (GSDMD-N) that triggers the formation of pores on the cell membrane and release of inflammatory cytokines interleukin(IL)-1β/18. Consequently, the pyroptotic death of cells causes inflammatory damage of the surrounding nerve cells.[7−10] The release of IL-1β has been observed in a kernicterus model rats.[11] Moreover, pyroptosis plays a crucial role in the pathogenesis of some neurological diseases, and inhibition of caspase-1 activation may be a potential intervention strategy.[12−14] VX-765, a specific caspase-1 inhibitor, has been used to control intractable epilepsy and some inflammatory diseases; in a phase II clinical trial of V-

Received: May 1, 2021
Accepted: July 12, 2021
Published: July 23, 2021

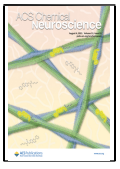

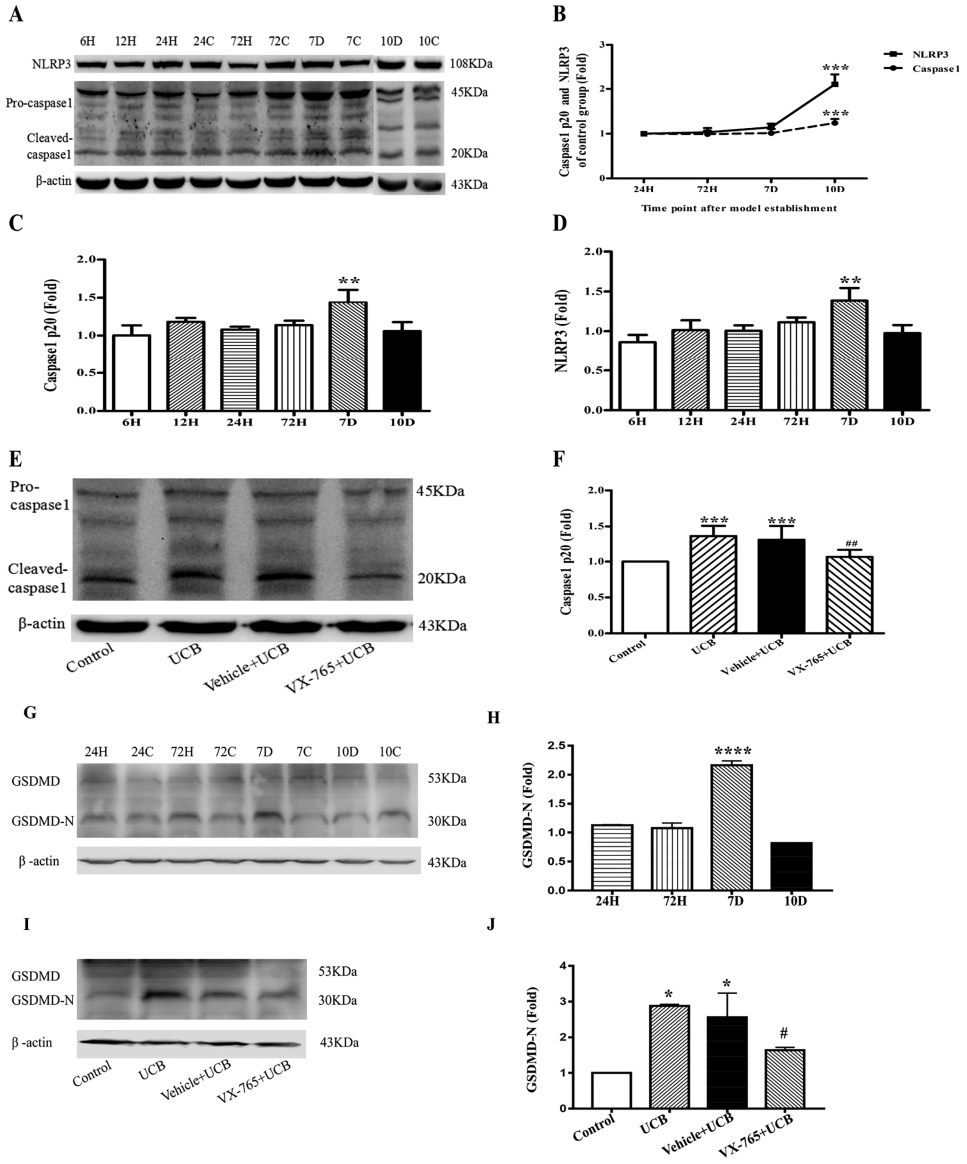

Figure 1. Expression levels of cleaved caspase-1 (p20), NLRP3, and GSDMD-N in the rat brain tissues of the different groups at different time points. Error bars represent the mean ± SD. (A) Protein expression of cleaved caspase-1 and NLRP3 in the brain tissue of the UCB and control groups were investigated by WB at different time points. (B) Expression levels of cleaved caspase-1 and NLRP3 in the brain tissue at different time points were detected. ***, $p < 0.001$ compared with 24 h control group; $n = 6$. (C) The comparisons of the cleaved caspase-1 expression compared with the control group, **, $p < 0.01$ compared with the corresponding control group, the cleaved caspase-1 expressed peaking at 7 days after the establishment of the model. $n = 6$. (D) The comparisons of the NLRP3 expression compared with the control group at corresponding time points, peaking at 7 days after the establishment of the model. **, $p < 0.01$ compared with the corresponding control group; $n = 6$. (E, F) VX-765+UCB group significantly attenuated the activation of caspase-1 at 7 days after the model was established. ***, $p < 0.001$ compared with the control group; ##, $p < 0.01$ compared with the UCB group ; $n = 8$. Quantification of the relative expression is normalized against the levels of β-actin. (G) Expression levels of cleaved GSDMD (GSDMD-N) in the brain tissue of the UCB and control groups were investigated by WB at different time points. (H) The comparisons of the GSDMD-N expression compared with the control group at corresponding time points, peaking at 7 days after the establishment of the model. ****, $p < 0.0001$ compared with the corresponding control group; $n = 5$. (I, J) VX-765+UCB group significantly attenuated the activation of GSDMD-N after the model was established. *, $p < 0.05$ compared with the control group; #, $p < 0.05$ compared with the UCB group; $n = 5$. Quantification of the relative expression is normalized against the levels of β-actin.

765, no severe adverse events were reported with its use for more than 6 weeks.[15−17] Furthermore, in a previous *in vitro* experiment, the inhibition of caspase-1 by VX-765 could partially reverse this UCB-induced neurotoxicity by preventing cell lysis (the formation of plasma membrane pores) and decreasing cytokines release in rat cortical astrocytes.[18] Therefore, the purpose of this study was to explore whether the pathogenesis of kernicterus was related to pyroptosis and whether VX-765 improved the short-term and long-term clinical outcomes of kernicterus model rats.

RESULTS AND DISCCUSSION

UCB Induced Activation of Whole Brain NLRP3, Caspase-1, and GSDMD-N in a Kernicterus Model Rat. First, the protein levels of cleaved caspase-1, p20 subunit (the activated form of caspase-1), and NLRP3 of rat brain at different time points were measured by Western blot. To

https://doi.org/10.1021/acschemneuro.1c00287
ACS Chem. Neurosci. 2021, 12, 2929−2939

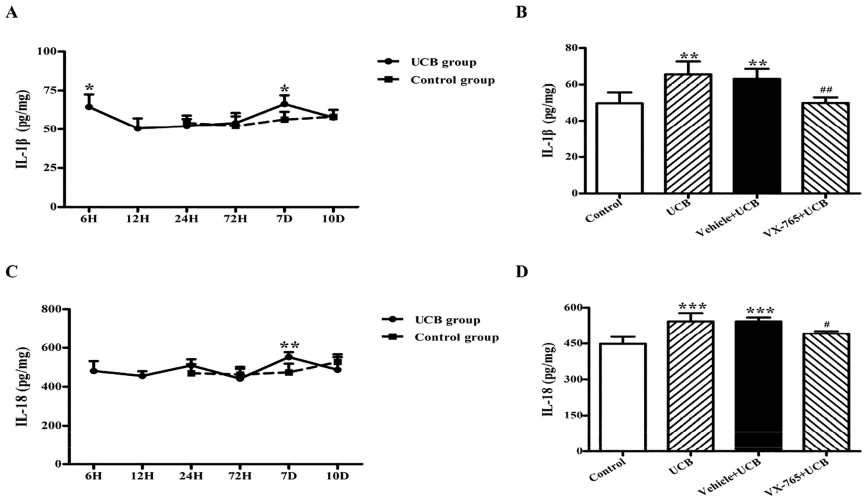

Figure 2. Release of IL-1β and IL-18 in rat whole brain tissues of the different groups at different time points (ELISA). Error bars represent the mean ± SD. (A) Release of IL-1β in the model rat brain tissue at different time points in the UCB and control groups. The peak time points of IL-1β secretion were 6 h and 7 days after modeling . *, $p < 0.05$ compared with the control group; $n = 5$. (B) Release of IL-1β in the brain tissue were significantly decreased in the rats of the VX-765+UCB group compared with that of the vehicle+UCB and of the UCB groups. **, $p < 0.01$ compared with the control group; ##, $p < 0.01$ compared with the UCB group; $n = 5$. (C) Release of IL-18 in the model rat brain tissue at different time points in the UCB and control groups. The peak time point of IL-18 secretion was 7 days after modeling. **, $p < 0.01$ compared with the corresponding control group; $n = 5$. (D) The levels of IL-18 in the brain tissue were significantly decreased in the rats of the VX-765+UCB group compared with those of the vehicle+UCB group and of the UCB group. ***, $p < 0.001$ compared with the control group; #, $p < 0.05$ compared with the UCB group; $n = 5$.

minimize the animal suffering and to ensure the same genetic background was used in every experiment, only one of each brood was chosen as the control group within 24 h. As time progressed, the expression of cleaved caspase-1 and NLRP3 of the control group markedly increased from postmodeling day 1 to day 10. On postmodeling day 10, the protein levels of cleaved caspase-1 and NLRP3 of the control group were significantly higher than the control group at postmodeling day 1 (both p values of <0.001, Figure 1B). Moreover, after standardization with the control group, the expression of NLRP3 (Figure 1A,D), cleaved caspase-1 (Figure 1A,C), and GSDMD-N (Figure 1G,H) of the model groups on postmodeling day 7 significantly increased ($p = 0.0011$, $p = 0.0012$, and $p < 0.0001$, respectively). The VX-765+UCB group significantly inhibited the activation of caspase-1 (Figure 1E,F) and GSDMD-N (Figure 1I,J) compared with the UCB group at 7 d ($p = 0.0013$ and $p = 0.0167$, respectively).

Caspase-1 Activation Mediated UCB-Induced Cytokines Release. To assess whether UCB-induced cytokines release was mediated by activated caspase-1, the levels of IL-1β and IL-18 were measured in the brain tissue of a newborn rat kernicterus model. To minimize the animal suffering and to ensure the same genetic background was used in every experiment, only one of each brood was chosen as the control within 24 h. The cytokines were released in a time-dependent manner (Figure 2A,C). IL-1β secretion began to increase at 6 h ($p = 0.0478$, compared with the control group) after the establishment of the model. From 12 to 72 h, the concentration of IL-1β decreased and showed no significant difference with the control group at the corresponding time point (at 24 and 72 h for the control group) and then reached the peak level at 7 d ($p = 0.0174$, compared with the control group). Similarly, IL-18 peaked at 7 d ($p = 0.009$, compared with the control group) after modeling and showed no significant difference with the control group at any corresponding time point. Furthermore, cytokine concentrations had almost no changes in the control group from postmodeling day 1 to day 10 (data not shown). Therefore, postmodeling day 7 was chosen as the representative time point for these two cytokines in the four different groups to investigate whether inhibition of caspase-1 activation reduced the release of cytokines in the kernicterus model rats. The results showed that the VX-765-pretreated rats significantly decreased the levels of IL-1β (Figure 2B) and IL-18 (Figure 2D) compared with the vehicle+UCB rats ($p = 0.0108$, $p = 0.0252$, respectively) and UCB rats ($p = 0.0026$, $p = 0.0242$, respectively).

Caspase-1 Activation Mediated UCB-Induced Morphological Injury and DNA Fragmentation. Since the cerebral cortex, hippocampus, and cerebellum are the regions that are susceptible to bilirubin neurotoxicity, these regions were chosen to analyze the pathological features in the experiment. Morphological alteration on postmodeling day 7 was measured by H&E staining (Figure 3A). Compared with the UCB group and the vehicle+UCB group, the cytoplasmic condensation and endolysis, nuclear pyknosis, karyorrhexis, and karyolysis were ameliorated in the VX-765+UCB group.

Meanwhile, UCB-induced DNA damage was examined by TUNEL staining (Figure 3B). The vehicle+UCB and UCB groups had a large number of TUNEL-positive cells in the cerebral cortex, hippocampus, and cerebellum compared with the control group, whereas the VX-765+UCB group only had a few positively stained cells in the brain. The rate of DNA fragmentation in the cortex was significantly reduced in the VX-765-pretreated rats (10.09 ± 0.79%) compared with those of the UCB group (23.12 ± 1.26%) and of the vehicle+UCB group (22.50 ± 1.05%) (both p values of <0.001) (Figure 3C). Similarly, the rate of DNA fragmentation in the hippocampus was markedly decreased in the VX-765-pretreated rats (11.84 ± 0.35%) compared with those of the UCB group (25.48 ± 2.19%) and of the vehicle+UCB group (24.79 ± 1.06%) (both p values of <0.001) (Figure 3D). Furthermore, the rate of

https://doi.org/10.1021/acschemneuro.1c00287
ACS Chem. Neurosci. 2021, 12, 2929−2939

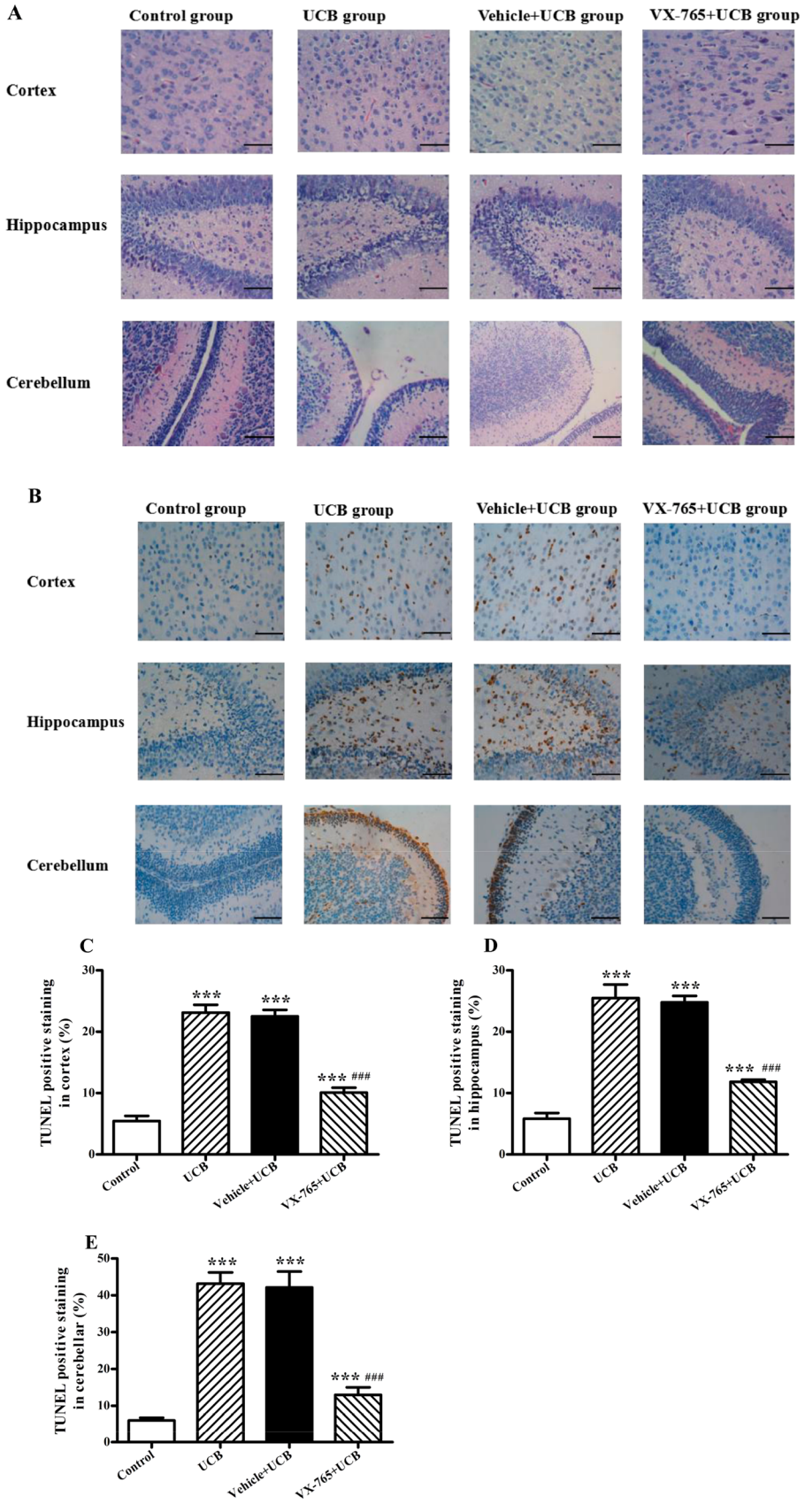

Figure 3. Images of cerebral cortex, hippocampus, and cerebellum of brain tissue in the different groups captured under light microscopy (H&E and TUNEL staining). Error bars represent the mean ± SD. (A) Morphological alteration on postmodeling day 7 was observed by H&E staining. Images of the H&E staining of four groups were captured using light microscopy. The UCB-induced cortical, hippocampal, and cerebellar neurons apparently exhibited cytoplasmic condensation, endolysis, nuclear pyknosis, karyorrhexis and karyolysis. However, the VX-765-treated group showed less damage. (Scale bars, 50 μm). (B) TUNEL staining was used on postmodeling day 7. Images of the TUNEL assay of four groups were

https://doi.org/10.1021/acschemneuro.1c00287
ACS Chem. Neurosci. 2021, 12, 2929−2939

Figure 3. continued

captured using light microscopy. The UCB group and vehicle+UCB group were obesrved more TUNEL-positive staining cells in the cerebral cortex, hippocampus, and cerebellum compared with the VX-765+UCB group. (Scale bars, 50 μm). (C−E) The DNA fragmentation rates were calculated based on randomly counting approximately 200 cells. The TUNEL-positive staining cell rates were significantly reduced in the VX-765-treated group compared with the UCB group and the vehicle+UCB group in the cerebral cortex, hippocampus and cerebellum. ***, $p < 0.001$ compared with the control group; ###, $p < 0.001$compared with the UCB group; $n = 4$.

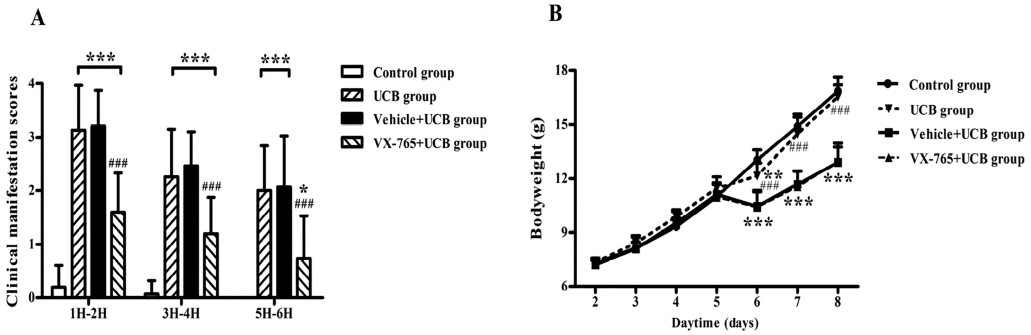

Figure 4. Rats' general condition (clinical manifestation scores) and body weights at different time points. Error bars represent the mean ± SD. (A) The clinical manifestations were scored every 2 h within the first 6 h after the treatment, the vehicle+UCB and UCB groups exhibited significantly higher scores than the VX-765+UCB group. *, $p < 0.05$, ***, $p < 0.001$ compared with the control group; ###, $p < 0.001$ compared with the UCB group; $n = 15$. (B) The body weights showed no significant differences between the VX-765+UCB group and the control group, whereas on day 6 after the model was established, the rat body weights in both the vehicle+UCB group and the UCB groups were significantly lower than the control group. **, $p < 0.01$, ***, $p < 0.001$ compared with the control group; ###, $p < 0.001$ compared with the UCB group; $n = 15$.

DNA fragmentation in the cerebellum was markedly attenuated in the VX-765-pretreated rats (12.99 ± 2.03%) compared with those of the UCB group (43.18 ± 3.03%) and of the vehicle+UCB group (42.13 ± 4.37%) (both p values of <0.001) (Figure 3E).

VX-765 Improved the General Condition of the Rats. The clinical manifestation score was assessed every 2 h within the first 6 h after the model was established (Figure 4A). In the vehicle+UCB, VX-765+UCB, and UCB groups, abnormal neurological manifestations, such as opisthotonus and latericumbent positioning, were observed, and the scores of these groups were markedly higher than the control group ($p < 0.001$). However, the score of the VX-765+UCB group was significantly lower than the vehicle+UCB group and the UCB group ($p < 0.001$).

The difference in body weight was not statistically significant among the four groups when the VX-765 or vehicle solution was injected from day 2 to day 5 after birth (Figure 4B). On postmodeling day 1 (day 6), the VX-765+UCB group showed significantly lower body weight than the control group ($p = 0.0012$); thereafter, there were no significant differences in weight gain between these two groups. Meanwhile, the body weight of the vehicle+UCB or of the UCB group was significantly lower than the control group after modeling($p < 0.001$).

The mortality was calculated for each group from postnatal day 5 (postmodeling day 0) to day 28. The VX-765-pretreated group had a significantly lower mortality rate of 17.65% compared with that of the UCB group (41.94%) and of the vehicle+UCB group (40.00%) ($p = 0.0394$ and 0.0472, respectively, χ^2 test, $n = 30-34$).

VX-765 Exerted Long-Term Neuroprotective Effects. The neurological evaluation system developed by Garcia et al. was used to observe the effect of VX-765 on the prognosis of nervous system in kernicterus model rats.[19] As shown in Figure 5A, the VX-765-pretreated rats demonstrated a significant improvement both in motor ability and in sensation function (scoring 15.89 ± 0.86) compared with the vehicle+UCB group (scoring 12.46 ± 0.45) and the UCB group (scoring 12.42 ± 1.00) (both p values of <0.001). More excitingly, there were no marked differences in neurological function between the VX-765+UCB group and the control group (scoring 16.47 ± 0.67).

A rotarod test was conducted to evaluate coordination and balance ability (Figure 5B). The residence time of the VX-765-pretreated rats (88.17 ± 8.32 s) was significantly higher than the vehicle+UCB rats (62.25 ± 7.21 s) and the UCB group rats (60.27 ± 7.39 s) (both p values of <0.001). What's more, there were no significant differences in the time spent on the apparatus between the VX-765+UCB group and the control group (91.82 ± 9.99 s).

An open field test was perfomed to assess the motor function (Figure 5C). The total 30 min movement distance of the four groups of rats was the following: the control group traveling 2620 ± 398.2 cm/30 min, the UCB group traveling 2676 ± 335.2 cm/30 min, the vehicle+UCB group traveling 2544 ± 298.5 cm/30 min, and the VX-765+UCB group traveling 2611 ± 329.5 cm/30 min. There was no statistical difference among all groups.

The Morris water maze was used to assess the spatial learning and memory capability of the rats. The tests detected motor function in the Morris water maze, and there were no obvious differences in the average swimming speed (Figure 5D(I)) and the daily swimming speed between the any two groups (Figure 5D(II)). To test the learning ability and memory, the VX-765+UCB group showed a shorter escape latency (6.99 ± 1.96 s) than the vehicle+UCB (14.27 ± 1.74 s) and UCB (15.93 ± 1.41 s) groups, (both p values of <0.001) on the sixth day, whereas no significant differences were found in escape latency compared with the control group (6.13 ± 2.46 s) (Figure 5D(III)). In addition, the vehicle+UCB rats (28.89 ± 11.93%) and the UCB rats (28.38 ± 7.14%) spent

https://doi.org/10.1021/acschemneuro.1c00287
ACS Chem. Neurosci. 2021, 12, 2929−2939

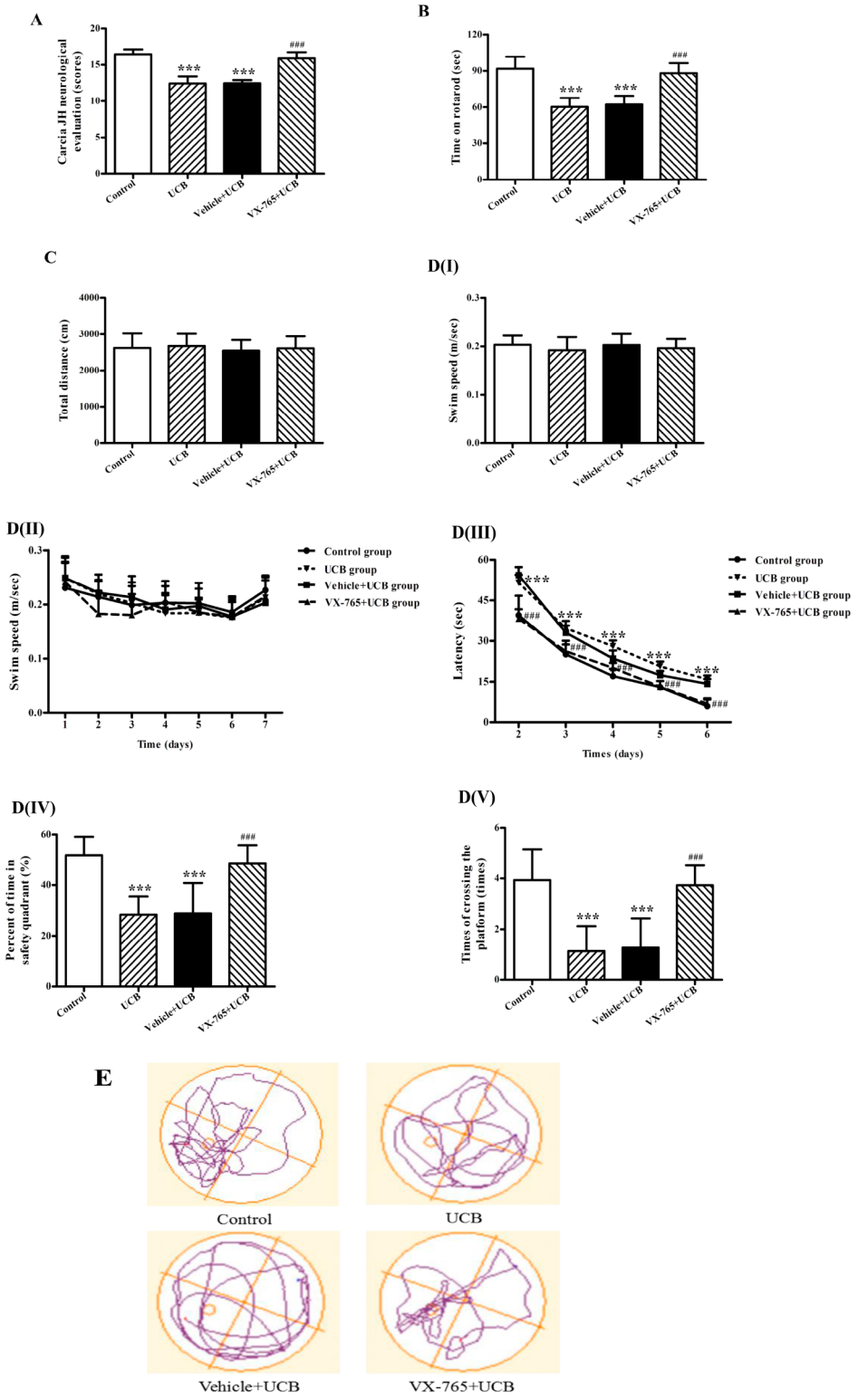

Figure 5. Assessments of the long-term neurological outcomes of the rats in the different groups. Error bars represent the mean ± SD: ***, $p < 0.001$ compared with the control group; ###, $p < 0.001$ compared with the UCB group. (A) Neurological function assessment system described by Garcia et al. The scores of the vehicle+UCB and the UCB groups were significantly lower than the VX-765+UCB group, whereas no significant differences were observed with the control group; $n = 11-15$. (B) Rotarod test. The vehicle+UCB and UCB groups spent less time on the accelerating rotarod than the VX-765+UCB group; no significant differences were observed with the control group; $n = 11-15$. (C) Open field test. The four groups were no significant differences in the total distance traveled in 30 min. $p > 0.05$ compared with the control group; $n = 11-15$. (D) Morris water maze. (I) Average swimming speed. The average swimming speed among the four groups were no significant differences. $p > 0.05$. (II) Daily swimming speed. There were no significant differences in the daily swimming speed over 7 days of testing among the four groups. $p > 0.05$. (III) Escape latency in the hidden-platform training. The rats in the VX-765+UCB group showed a shorter latency for escape onto the platform than the vehicle+UCB and the UCB group, whereas no significant differences were observed with the control group. ***, $p < 0.001$ compared with the control group; ###, $p < 0.001$ compared with the UCB group. (IV) The percentage of time spent in the safety quadrant during

https://doi.org/10.1021/acschemneuro.1c00287
ACS Chem. Neurosci. 2021, 12, 2929−2939

Figure 5. continued

the probe trial of the Morris water maze. The vehicle+UCB and UCB groups spent less time in the safety quadrant than the VX-765-treated rats, without significant differences from the control group. (V) The number of times that the rats crossed over the platform in the probe trial of the Morris water maze. The VX-765-treated rats crossed over the platform more times than the vehicle+UCB and UCB groups, without significant differences from those of the control group. (E) Representative swimming paths of the four groups during the probe trial of the Morris water maze. For Morris water maze testing, n = 11−15.

less time in the safety quadrant than the VX-765-pretreated rats (48.48 ± 7.34%) (both p values of <0.001), whereas no significant differences in time spent in the safety quadrant were found compared with the control group (51.68 ± 7.44%) (Figure 5D(IV)). Furthermore, there were obvious increases in the number of times the rats crossed the platform location in the VX-765-pretreated rats compared with the vehicle+UCB group and the UCB group, (3.73 ± 0.79) versus (1.27 ± 1.16) and (1.13 ± 0.99) (both p values <0.001), respectively, whereas the number of times that the VX-765-pretreated rats crossed over the platform was similar to the control group (3.93 ± 1.22) (Figure 5D(V)).

Neuroinflammation, a basic immune response of the brain in response to a variety of exogenous pathogens and host-derived injury signals, has been identified to be involved in the pathogenesis of various neurological diseases. At present, an increasing number of studies have demonstrated that inflammation plays a critical role in neurological diseases, especially in the injury of the developing brain, which is closely related to perinatal neuroinflammation, possibly causing higher susceptibility to various neurodegenerative diseases in adulthood.[20] In the nervous system, neuroinflammation can be initiated through the activation of glial cells and cytokines release in response to invading agents, which could promote tissue repair and exert a neuroprotective function. However, excessive inflammation may lead to tissue damage.[20−23] Kernicterus is a type of permanent neurological dysfunction due to prolonged exposure of the brain to high-level UCB, which can be life-threatening.[24] Previous studies have confirmed that the neurotoxicity of UCB not only induced nerve cell death but was also closely related to the inflammation of neural tissues.[3,4,25] Pyroptosis is a mode of death involving swelling and lysis of cells, which leads to the release of a large amount of cell content and then triggers strong inflammation.[26] In recent years, pyroptosis is considered to be related to the occurrence and development of several nervous system diseases, including brain infection, trauma, and chronic neurodegenerative diseases.[7,13,14,27] Many research groups proved that inflammasomes, particularly NLRP3, were responsible for the activation of caspase-1 and the secretion of inflammatory cytokines, triggering pyroptosis and other inflammatory responses.[8] NLRP3 is abundantly expressed in CNS diseases in response to various exogenous pathogens, such as bacteria and viruses, and to endogenous signals, such as ATP, uric acid, and amyloid.[7,22,28,29] In this study, UCB induced the upregulation of the NLRP3 protein in the brain of the kernicterus model rats, consistent with the location of activated caspase-1, which was time-dependent and peaked at 7 d after the model was established. The elevated levels of NLRP3 and activated caspase-1 suggested that the NLRP3 inflammasome pathway might be involved in UCB-induced pyroptosis *in vivo*. Inflammatory caspases can cleave the domain between the N-terminal and C-terminal of GSDMD. GSDMD, or more accurately, its N-terminal, is enough to cause pyroptosis, regardless of the cellular system.[10,26,30] This study demonstrated that UCB activated GSDMD dependent pyroptosis, coinciding with the peak time of caspase-1 activation.

Meanwhile, the levels of IL-1β and IL-18 were increased when caspase-1 activation peaked. However, IL-1β is a strong proinflammatory factor; the amounts of secreted IL-1β were low in the early stage of the model, which may be related to the anti-inflammatory function of microglia, such as IL-10, limiting IL-1β release.[31,32] Conversely, 7 d later, the model established the peak of inflammatory factor release, speculating the progression of inflammatory damage. Moreover, the secretion of IL-18 easily prolongs inflammation and causes the occurrence of chronic inflammation.[33] Consistent with the control cortical impact injury model, proinflammatory microglia cells were mainly expressed after 7 d.[31] At this time, microglia are not enough to limit the damage. Astrocytes are also considered to have damage and protective effects. In multiple sclerosis, the astrocytes were depleted in the early stage to aggravate the course of the disease, while they were knocked out in the later stage to improve the clinical outcomes.[34] Overall, these studies show that microglia and astrocytes play a major role in maintaining brain balance in the early stages of the disease, while in the long run, their contribution to harmful neuroinflammatory responses is major.

It has been widely accepted that the activation of pro-IL-1β and pro-IL-18 into mature inflammatory cytokines is catalyzed by activated caspase-1, while GSDMD cannot hydrolyze IL-1β/18 to make them mature. GSDMD is the substrate of caspase-1, and its N-terminal is cut off during the activation of caspase-1, and this cleavage is necessary for pyroptosis and IL-1β/18 secretion, so local inflammatory response is induced by the formation of pores in the cell membrane.[35,36] Eventually, DNA cleavage in the pyroptosis process results in cell death.[7] When caspase-1 and GSDMD were activated at 7 d after the model was established, increased DNA cleavage was detected in the regions that are susceptible to bilirubin, suggesting that caspase-1 activation and pyroptosis were most likely involved in the pathogenesis of UCB neurotoxicity. Thus, we examined whether the administration of VX-765 exerted neuroprotective effects through the inhibition of the caspase-1-GSDMD pathway. Maroso et al.[37] and Ravizzaet et al.[38] reported that systemic injection of VX-765 significantly reduced seizure activity by inhibiting the release of the inflammatory cytokine IL-1β. In addition, Heneka et al.[39] and Tan et al.[12] reported that by silencing caspase-1 in a mouse AD model, the clearance rate of β-amyloid protein, the major pathogenic factor of AD, was enhanced, and the cognitive impairment and the other related neurological sequelae of the model animals were evidently attenuated. Clearly, in the study, UCB activates caspase-1, the latter then cleaved GSDMD, leading to increased cytokines release and DNA fragmentation. VX-765-pretreatment decreased the activation of caspase-1 and GSDMD-N and preserved the neurons' morphology in the cortex, hippocampus, and cerebellum. In addition, the VX-765-pretreated rats exhibited less abnormal neurological manifes-

https://doi.org/10.1021/acschemneuro.1c00287
ACS Chem. Neurosci. 2021, 12, 2929−2939

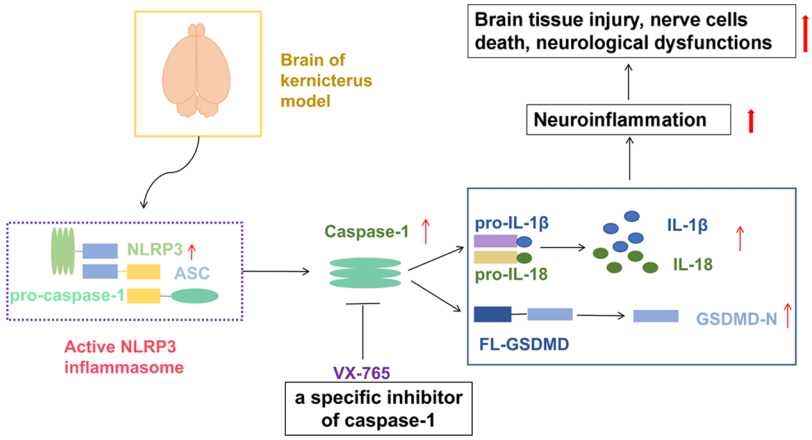

Figure 6. Proposed mechanism of UCB induced neurotoxicity and VX-765 in the intervention of kernicterus.

tations and lower mortality than the untreated model rats, similar to the achievement of minocycline reported in UGT1$^{-/-}$ mice.[4] Thus, VX-765 exerted a neuroprotective effect for UCB-related neurotoxicity, which might be a potential treatment for kernicterus.

Early bilirubin exposure causes long-term memory and balance abnomalities, whose functional regions are both susceptible to bilirubin, such as the cerebellum and hippocampus.[40] Similarly, 3 days of bilirubin exposure on newborn rat induced Alzheimer's disease like pathological behavior later on.[41] Thus, a series of behavioral tests were also conducted to evaluate the effect of VX-765 on the long-term neurological outcomes of the model rats. The VX-765-pretreated kernicterus rats achieved significantly better performance both in fine motor ability and in sensitive function than that of the untreated model group and improved the motor and balance ability. Likewise, as a major component of the limbic system, the hippocampus plays a crucial role in cognitive development, especially in spatial learning and memory, which enables navigation.[42] The VX-765-pretreated group demonstrated improved learning and memory compared with that of the untreated model group in the Morris water maze. In short, VX-765 treatment improved the long-term behavioral ability of model rats.

Taken together, this study employed the kernicterus rat model to prove that pyroptosis is involved in the pathogenesis of bilirubin encephalopathy. Additionally, the inhibition of caspase-1 activation by VX-765 could partially reverse the UCB-induced neurotoxicity, exerting a neuroprotective effect not only in the acute phase but also in the chronic phase of kernicterus. It is reasonable to hypothesize that the inhibition of the pyroptosis pathway could be a potential treatment option for the prevention of kernicterus. Figure 6 summarized the proposed mechanism of VX-765 in the intervention of kernicterus.

METHODS

Experimental Animals. Experimental SPF Sprague-Dawley rats were purchased from the Animal Experimental Center of Chongqing Medical University. All animal experiments are conducted in accordance with the guidelines specified by the Animal experiment Management Committee and approved by the Ethics Committee of Chongqing Medical University (license number SYXK2007-0016). The rats were exposed to a 23 ± 2 °C environment and 12 h/12 h light/dark cycle and were free to eat and drink.

Animal Treatment and Model Establishment. At postnatal day 2, the rat pups were randomly divided into four groups (as described above): control group, UCB group, vehicle+UCB group, and VX-765+UCB group. VX-765 (Selleck Chemicals), dissolved in 2% DMSO in 30% PEG-300 (Sigma-Aldrich) in double-distilled water, was injected at 50 mg/kg intraperitoneally in VX-765+UCB group of rats daily (i.e., at 10:00 a.m.) for 4 consecutive days, whereas those of the control group and of vehicle+UCB group were intraperitoneally administered equal volumes of DMSO, PEG-300, and double-distilled water. At postnatal day 5, the last injection was done at 45 min before kernicterus model was established, and the vehicle+UCB group, VX-765+UCB group, and UCB group were given an injection of bilirubin solution 10 μg/g (body weight). The control group was given an injection of equal volumes of double-distilled water (pH = 8.5).

The establishment method of the rat kernicterus model was the same as described previously.[43] The Sprague-Dawley rat pups (10−15 g) were anesthetized with diethyl ether. Then, release of the cerebrospinal fluid from the cisterna magna was done using a microinjector. Finally, the bilirubin solution was injected into cistern magna, and the control group was injected with the same amount of control solution. The bilirubin (Sigma-Aldrich) was dissolved in a 0.5 M NaOH solution, the mixture was diluted in double-distilled H_2O, and the pH was adjusted with HCl (0.5 M) to 8.5, the sample finally prepared as a transparent orange solution (10 mg/mL).[44]

A total of 265 rats were used, regardless of gender. From the 1st to 10th day after the model establishment, animals of control and UCB group were euthanized and whole brain tissues were collected for WB and ELISA. At 7th day after the model establishment, animals of four groups were euthanized and whole brain tissues were collected for WB, ELISA, and histology staining. At postnatal day 28, the mortality was calculated, while behavioral experiments were performed which included the animals' conformance to modeling standard and excluded animals unable to complete the tests.

Western Blotting (WB). The total protein of brain tissue was extracted by NP-40 lysate (Beyotime Biotechnology) containing complete protease inhibitor PMSF (1 mM) (Beyotime Biotechnology), and the BCA method (Beyotime Biotechnology) was used to determin the ptotein concentrations. The 12% SDS−PAGE gel was prepared, and the sample was added according to the protein concentration. After electrophoresis, the protein was transferred to PVDF membrane and then sealed with 5% skim milk at room temperature for 1 h. The primary antibody (anti-caspase-1, anti-NLRP3, or anti-β-actin, all at 1:500, Abcam; anti-GSDMD, 1:1000, Abbexa) was incubated overnight in a 4° shaking table. The secondary antibody (all at 1:1000, Cell Signaling Technology) was incubated at room temperature for 1 h, and ECL assay kit (Bio-Rad) was used to visualize the protein bands.

ELISA. Total protein of brain tissue was extracted from NP40 lysate (Beyotime Biotechnology), and the operation was performed

https://doi.org/10.1021/acschemneuro.1c00287
ACS Chem. Neurosci. 2021, 12, 2929−2939

according to the instructions of the ELISA kit (RayBiotech). The absorbance value at 450 nm of each well was detected by microplate (BioTek), and the standard curve was established and calculated. Then, the levels of the IL-1β and IL-18 proteins were measured. Each sample was measured in duplicate.

Histology. After 7 days of modeling, the brains of rats in each group were sacrificed and fixed with 4% paraformaldehyde. After paraffin embedding, the cortex, hippocampus (cornu ammonis 1 (CA1), CA2, and CA3), and cerebellar paraffin slices (4 mm) were cut. Hematoxylin−eosin (H&E) and terminal deoxynucleotidyl-transferase-mediated nick end labeling (TUNEL) staining (Roche Applied Science) were conducted according to the instructions. The morphological alternation in the hippocampus, cerebral cortex, and cerebellum were observed by light microscopy (Nikon).

Dynamic Assessment of the Clinical Manifestations. After modeling, the following typical neurological manifestations of bilirubin encephalopathy were observed every 1 h, including clenched fists, opisthotonus, latericumbent positioning, and rolling. Any manifestation would be scored one point, which is recorded 3 times within 6 h after modeling. The clinical manifestations were measured by the double-blind method.[43]

Body Weights. The body weight was daily recorded from the second day after birth up until the third day after the model establishment (day 2 to day 8 after birth).

Mortality. The mortality of rats in each group was recorded for 28 consecutive days after the model establishment.

Neurological Evaluation. The neurological function was assessed at postnatal 28 using the neurological evaluation system described by Garcia et al.,[19] which included spontaneous activity, climbing, forepaw outstretching, symmetry in the movement of the four limbs, body proprioception, and response to vibrissae touch. With a full score of 18, the lower the score, the more serious is the neurological damage. The neurological functions were measured by the double-blind method.

Rotarod Test. At the age of 28 days, the rotatod test was carried out to detect the ability of coordination and balance. The rats were acclimatized to the environment and instrument 1 day in advance. The experimental rats were placed on the equipment, and the rotational speed was increased from 10 to 80 rpm. The test was carried out every 3 min, from the rats staying on the rotating rod until it fell off or ended for 3 min. The exercise time of each rat was recorded when the rats fell off the rotating rod, and the experiment was repeated 4 times for each rat, and the average time was calculated.

Open Field Test. The open field test was used to observe the mobility of 28-day-old rats. The rats in each group were placed in the center of a square field (60 cm × 60 cm × 60 cm) and allowed to move freely for 30 min. ANY-maze software was used to record video and data and to measure the distance of walking in 30 min to reflect the animal's mobility.[45]

Morris Water Maze. The spatial learning and memory abilities of the rats were evaluated using the Morris water maze at 28 days.[11] Briefly, a water maze consists of a circular pool filled with black ink (25 ± 1 °C). The experiment lasted for 7 days. The first day was adaptive training, and the platform training was removed once. During the positioning navigation training on days 2−6, the experimental rats were put into water. If the platform was not found over 60 s, the animals were guided to the platform and stayed there for 10 s. Each experimental rat was trained 4 times a day with at least 15−20 min interval between training sessions. On the seventh day, the platform was removed and a probe test was carried out in 60 s. The experimental animals were put into the water from the opposite side of the platform quadrant, and the searching time of the experimental animals in the target quadrant and the times of crossing the platform were recorded within 60 s.

Statistical Analysis. The data were statistically analyzed by Prism package (GraphPad Software, La Jolla, CA, USA) and were presented as the mean ± standard deviation. After the data were tested by the normality and variance homogeneity test, the significant differences between groups were analyzed by an ANOVA with Bonferroni's post-test. The categorical data were analyzed by χ^2 test. A p value of <0.05 was consider statistically significant.

AUTHOR INFORMATION

Corresponding Author

Ziyu Hua − *Department of Neonatology, Children's Hospital of Chongqing Medical University, Ministry of Education Key Laboratory of Child Development and Disorders, Chongqing 400014, China; China International Science and Technology Cooperation Base of Child Development and Critical Disorders, Chongqing 400014, China*; Phone: 86-23-63633044; Email: h_ziyu0517@163.com

Authors

Siyu Li − *Department of Neonatology, Children's Hospital of Chongqing Medical University, Ministry of Education Key Laboratory of Child Development and Disorders, Chongqing 400014, China; China International Science and Technology Cooperation Base of Child Development and Critical Disorders, Chongqing 400014, China; Chongqing Key Laboratory of Child Infection and Immunity, Chongqing 400014, China*

Hongmei Huang − *Department of Neonatology, Children's Hospital of Chongqing Medical University, Ministry of Education Key Laboratory of Child Development and Disorders, Chongqing 400014, China; China International Science and Technology Cooperation Base of Child Development and Critical Disorders, Chongqing 400014, China; Chongqing Key Laboratory of Child Infection and Immunity, Chongqing 400014, China*; orcid.org/0000-0003-1158-7911

Qian Wei − *Department of Neonatology, Children's Hospital of Chongqing Medical University, Ministry of Education Key Laboratory of Child Development and Disorders, Chongqing 400014, China; China International Science and Technology Cooperation Base of Child Development and Critical Disorders, Chongqing 400014, China; Chongqing Key Laboratory of Child Infection and Immunity, Chongqing 400014, China*

Chunmei He − *Department of Neonatology, Children's Hospital of Chongqing Medical University, Ministry of Education Key Laboratory of Child Development and Disorders, Chongqing 400014, China; China International Science and Technology Cooperation Base of Child Development and Critical Disorders, Chongqing 400014, China; Chongqing Key Laboratory of Child Infection and Immunity, Chongqing 400014, China*

Jie Feng − *Department of Neonatology, Children's Hospital of Chongqing Medical University, Ministry of Education Key Laboratory of Child Development and Disorders, Chongqing 400014, China*

Yao Wang − *Department of Neonatology, Children's Hospital of Chongqing Medical University, Ministry of Education Key Laboratory of Child Development and Disorders, Chongqing 400014, China*

Mengwen Li − *Department of Neonatology, Children's Hospital of Chongqing Medical University, Ministry of Education Key Laboratory of Child Development and Disorders, Chongqing 400014, China*

Qiannan Zhang − *Department of Neonatology, Children's Hospital of Chongqing Medical University, Ministry of Education Key Laboratory of Child Development and Disorders, Chongqing 400014, China; China International*

https://doi.org/10.1021/acschemneuro.1c00287
ACS Chem. Neurosci. 2021, 12, 2929−2939

Science and Technology Cooperation Base of Child Development and Critical Disorders, Chongqing 400014, China

Xuhua Xia − *Department of Neonatology, Children's Hospital of Chongqing Medical University, Ministry of Education Key Laboratory of Child Development and Disorders, Chongqing 400014, China; China International Science and Technology Cooperation Base of Child Development and Critical Disorders, Chongqing 400014, China*

Complete contact information is available at: https://pubs.acs.org/10.1021/acschemneuro.1c00287

Author Contributions

Z.H., S.L., H.H., and Q.W. conceived and designed the experiments. H.H., Q.W., S.L., C.H., and J.F. performed the experiments. Z.H., S.L., H.H., Q.W., S.L., C.H., and J.F. analyzed the data. X.X., Q.W., H.H., S.L., C.H., J.F., Y.W., and M.L. contributed to the materials/reagents/analysis tools. Z.H., S.L., H.H., Q.W., X.X., C.H., and Q.Z. wrote the paper. All authors read and approved the final manuscript.

Funding

This work was supported by the National Natural Science Foundation of China (Grant 81971426) and the Project of Basic and Frontier Research Plan of Chongqing (Grant CSTC2018jcyjAX0284).

Notes

The authors declare no competing financial interest.

■ ACKNOWLEDGMENTS

We are grateful to Yan Zhang for the excellent technical assistance during the experiments.

■ REFERENCES

(1) Olusanya, B. O., Ogunlesi, T. A., and Slusher, T. M. (2014) Why is kernicterus still a major cause of death and disability in low-income and middle-income countries. *Arch. Dis. Child. 99*, 1117−1121.

(2) Greco, C., Arnolda, G., Boo, N. Y., Iskander, I. F., Okolo, A. A., Rohsiswatmo, R., Shapiro, S. M., Watchko, J., Wennberg, R. P., Tiribelli, C., and Coda Zabetta, C. D. (2016) Neonatal Jaundice in Low- and Middle-Income Countries: Lessons and Future Directions from the 2015 Don Ostrow Trieste Yellow Retreat. *Neonatology 110*, 172−180.

(3) Vodret, S., Bortolussi, G., Jašprová, J., Vitek, L., and Muro, A. F. (2017) Inflammatory signature of cerebellar neurodegeneration during neonatal hyperbilirubinemia in Ugt1 (-/-) mouse model. *J. Neuroinflammation 14*, 64.

(4) Vodret, S., Bortolussi, G., Iaconcig, A., Martinelli, E., Tiribelli, C., and Muro, A. F. (2018) Attenuation of neuro-inflammation improves survival and neurodegeneration in a mouse model of severe neonatal hyperbilirubinemia. *Brain, Behav., Immun. 70*, 166−178.

(5) Geiger, A. S., Rice, A. C., and Shapiro, S. M. (2007) Minocycline blocks acute bilirubin-induced neurological dysfunction in jaundiced Gunn rats. *Neonatology 92*, 219−226.

(6) Liaury, K., Miyaoka, T., Tsumori, T., Furuya, M., Hashioka, S., Wake, R., Tsuchie, K., Fukushima, M., Limoa, E., Tanra, A. J., and Horiguchi, J. (2014) Minocycline improves recognition memory and attenuates microglial activation in Gunn rat: a possible hyperbilirubinemia-induced animal model of schizophrenia. *Prog. Neuro-Psychopharmacol. Biol. Psychiatry 50*, 184−190.

(7) Bergsbaken, T., Fink, S. L., and Cookson, B. T. (2009) Pyroptosis: host cell death and inflammation. *Nat. Rev. Microbiol. 7*, 99−109.

(8) Lamkanfi, M., and Dixit, V. M. (2014) Mechanisms and functions of inflammasomes. *Cell 157*, 1013−1022.

(9) Liu, X., Zhang, Z. B., Ruan, J. B., Pan, Y. D., Magupalli, V. G., Wu, H., and Lieberman, J. (2016) Inflammasome-activated gasdermin D causes pyroptosis by forming membrane pores. *Nature 535*, 153−8.

(10) Shi, J. J., Zhao, Y., Wang, K., Shi, X. Y., Wang, Y., Huang, H. W., Zhuang, Y. H., Cai, T., Wang, F. C., and Shao, F. (2015) Cleavage of GSDMD by inflammatory caspases determines pyroptotic cell death. *Nature 526*, 660−5.

(11) Li, M. W., Song, S. J., Li, S. J., Feng, J., and Hua, Z. Y. (2015) The Blockade of NF-kappaB Activation by a Specific Inhibitory Peptide Has a Strong Neuroprotective Role in a Sprague-Dawley Rat Kernicterus Model. *J. Biol. Chem. 290*, 30042−52.

(12) Tan, C. C., Zhang, J. G., Tan, M. S., Chen, H., Meng, D. W., Jiang, T., Meng, X. F., Li, Y., Sun, Z., Li, M. M., Yu, J. T., and Tan, L. (2015) NLRP1 inflammasome is activated in patients with medial temporal lobe epilepsy and contributes to neuronal pyroptosis in amygdala kindling-induced rat model. *J. Neuroinflammation 12*, 18.

(13) Tan, M. S., Tan, L., Jiang, T., Zhu, X. C., Wang, H. F., Jia, C. D., and Yu, J. T. (2014) Amyloid-beta induces NLRP1-dependent neuronal pyroptosis in models of Alzheimer's disease. *Cell Death Dis. 5*, e1382.

(14) Liu, W., Chen, Y., Meng, J., Wu, M., Bi, F., Chang, C., Li, H., and Zhang, L. (2018) Ablation of caspase-1 protects against TBI-induced pyroptosis in vitro and in vivo. *J. Neuroinflammation 15*, 48.

(15) Doitsh, G., Galloway, N. L., Geng, X., Yang, Z., Monroe, K. M., Zepeda, O., Hunt, P. W., Hatano, H., Sowinski, S., Muñoz-Arias, I., and Greene, W. C. (2014) Cell death by pyroptosis drives CD4 T-cell depletion in HIV-1 infection. *Nature 505*, 509−514.

(16) Kang, R., Zeng, L., Zhu, S., Xie, Y., Liu, J., Wen, Q., Cao, L., Xie, M., Ran, Q., Kroemer, G., Wang, H., Billiar, T. R., Jiang, J., and Tang, D. (2018) Lipid Peroxidation Drives Gasdermin D-Mediated Pyroptosis in Lethal Polymicrobial Sepsis. *Cell Host Microbe 24*, 97−108.

(17) Wannamaker, W., Davies, R., Namchuk, M., Pollard, J., Ford, P., Ku, G., Decker, C., Charifson, P., Weber, P., Germann, U. A., Kuida, K., and Randle, J. C. (2007) (S)-1-((S)-2-{[1-(4-amino-3-chloro-phenyl)-methanoyl]-amino}-3,3-dimethyl-butanoy l)-pyrrolidine-2-carboxylic acid ((2R,3S)-2-ethoxy-5-oxo-tetrahydro-furan-3-yl)-amide (VX-765), an orally available selective interleukin (IL)-converting enzyme/caspase-1 inhibitor, exhibits potent anti-inflammatory activities by inhibiting the release of IL-1beta and IL-18. *J. Pharmacol. Exp. Ther. 321*, 509−516.

(18) Feng, J., Li, M., Wei, Q., Li, S., Song, S., and Hua, Z. (2018) Unconjugated bilirubin induces pyroptosis in cultured rat cortical astrocytes. *J. Neuroinflammation 15*, 23.

(19) Garcia, J. H., Wagner, S., Liu, K. F., and Hu, X. J. (1995) Neurological deficit and extent of neuronal necrosis attributable to middle cerebral artery occlusion in rats. Statistical validation. *Stroke 26*, 627−634 (discussion 635).

(20) Hagberg, H., Mallard, C., Ferriero, D. M., Vannucci, S. J., Levison, S. W., Vexler, Z. S., and Gressens, P. (2015) The role of inflammation in perinatal brain injury. *Nat. Rev. Neurol. 11*, 192−208.

(21) Hagberg, H., Gressens, P., and Mallard, C. (2012) Inflammation during fetal and neonatal life: implications for neurologic and neuropsychiatric disease in children and adults. *Ann. Neurol. 71*, 444−457.

(22) Song, L., Pei, L., Yao, S., Wu, Y., and Shang, Y. (2017) NLRP3 Inflammasome in Neurological Diseases, from Functions to Therapies. *Front. Cell. Neurosci. 11*, 63.

(23) Xanthos, D. N., and Sandkühler, J. (2014) Neurogenic neuroinflammation: inflammatory CNS reactions in response to neuronal activity. *Nat. Rev. Neurosci. 15*, 43−53.

(24) Watchko, J. F., and Tiribelli, C. (2013) Bilirubin-induced neurologic damage−mechanisms and management approaches. *N. Engl. J. Med. 369*, 2021−2030.

(25) Brites, D. (2012) The evolving landscape of neurotoxicity by unconjugated bilirubin: role of glial cells and inflammation. *Front. Pharmacol. 3*, 88.

(26) Ding, J. J., Wang, K., Liu, W., She, Y., Sun, Q., Shi, J. J., Sun, H. Z., Wang, D. C., and Shao, F. (2016) Pore-forming activity and structural autoinhibition of the gasdermin family. *Nature 535*, 111−6.
(27) Zhou, K., Shi, L., Wang, Y., Chen, S., and Zhang, J. (2016) Recent Advances of the NLRP3 Inflammasome in Central Nervous System Disorders. *J. Immunol. Res. 2016*, 9238290.
(28) Saresella, M., La Rosa, F., Piancone, F., Zoppis, M., Marventano, I., Calabrese, E., Rainone, V., Nemni, R., Mancuso, R., and Clerici, M. (2016) The NLRP3 and NLRP1 inflammasomes are activated in Alzheimer's disease. *Mol. Neurodegener. 11*, 23.
(29) Man, S. M., Karki, R., and Kanneganti, T. D. (2017) Molecular mechanisms and functions of pyroptosis, inflammatory caspases and inflammasomes in infectious diseases. *Immunol. Rev. 277*, 61−75.
(30) Yang, Y., Liu, P. Y., Bao, W., Chen, S. J., Wu, F. S., and Zhu, P. Y. (2020) Hydrogen inhibits endometrial cancer growth via a ROS/NLRP3/caspase-1/GSDMD-mediated pyroptotic pathway. *BMC Cancer 20*, 28.
(31) Morganti-Kossmann, M. C., Semple, B. D., Hellewell, S. C., Bye, N., and Ziebell, J. M. (2019) The complexity of neuroinflammation consequent to traumatic brain injury: from research evidence to potential treatments. *Acta Neuropathol. 137*, 731−755.
(32) Pachathundikandi, S. K., and Backert, S. (2018) Helicobacter pylori controls NLRP3 expression by regulating hsa-miR-223-3p and IL-10 in cultured and primary human immune cells. *Innate Immun. 24*, 11−23.
(33) Sedimbi, S. K., Hägglöf, T., Garimella, M. G., Wang, S., Duhlin, A., Coelho, A., Ingelshed, K., Mondoc, E., Malin, S. G., Holmdahl, R., Lane, D. P., Leadbetter, E. A., and Karlsson, M. C. I. (2020) Combined proinflammatory cytokine and cognate activation of invariant natural killer T cells enhances anti-DNA antibody responses. *Proc. Natl. Acad. Sci. U. S. A. 117*, 9054−9063.
(34) Brambilla, R. (2019) The contribution of astrocytes to the neuroinflammatory response in multiple sclerosis and experimental autoimmune encephalomyelitis. *Acta Neuropathol. 137*, 757−783.
(35) Evavold, C. L., Ruan, J. B., Tan, Y. H., Xia, S. Y., Wu, H., and Kagan, J. C. (2018) The Pore-Forming Protein Gasdermin D Regulates Interleukin-1 Secretion from Living Macrophages. *Immunity 48*, 35−44.
(36) He, W. T., Wan, H. Q., Hu, L. C., Chen, P. D., Wang, X., Huang, Z., Yang, Z. H., Zhong, C. Q., and Han, J. H. (2015) Gasdermin D is an executor of pyroptosis and required for interleukin-1βsecretion. *Cell Res. 25*, 1285−98.
(37) Maroso, M., Balosso, S., Ravizza, T., Iori, V., Wright, C. I., French, J., and Vezzani, A. (2011) Interleukin-1beta biosynthesis inhibition reduces acute seizures and drug resistant chronic epileptic activity in mice. *Neurotherapeutics 8*, 304−315.
(38) Ravizza, T., Noé, F., Zardoni, D., Vaghi, V., Sifringer, M., and Vezzani, A. (2008) Interleukin Converting Enzyme inhibition impairs kindling epileptogenesis in rats by blocking astrocytic IL-1beta production. *Neurobiol. Dis. 31*, 327−333.
(39) Heneka, M. T., Kummer, M. P., Stutz, A., Delekate, A., Schwartz, S., Vieira-Saecker, A., Griep, A., Axt, D., Remus, A., Tzeng, T. C., Gelpi, E., Halle, A., Korte, M., Latz, E., and Golenbock, D. T. (2013) NLRP3 is activated in Alzheimer's disease and contributes to pathology in APP/PS1 mice. *Nature 493*, 674−678.
(40) Watchko, J. F. (2006) Kernicterus and the molecular mechanisms of bilirubin-induced CNS injury in newborns. *NeuroMol. Med. 8*, 513−529.
(41) Chen, H., Liang, L., Xu, H., Xu, J., Yao, L., Li, Y., Tan, Y., Li, X., Huang, Q., Yang, Z., Wu, J., Chen, J., Huang, H., Wang, X., Zhang, C. E., and Liu, J. (2020) Short Term Exposure to Bilirubin Induces Encephalopathy Similar to Alzheimer's Disease in Late Life. *J. Alzheimer's Dis. 73*, 277−295.
(42) Rossato, J. I., Bevilaqua, L. R., Myskiw, J. C., Medina, J. H., Izquierdo, I., and Cammarota, M. (2007) On the role of hippocampal protein synthesis in the consolidation and reconsolidation of object recognition memory. *Learn. Mem. 14*, 36−46.
(43) Song, S., Hu, Y., Gu, X., Si, F., and Hua, Z. (2014) A novel newborn rat kernicterus model created by injecting a bilirubin solution into the cisterna magna. *PLoS One 9*, e96171.
(44) Wennberg, R. P., and Hance, A. J. (1986) Experimental bilirubin encephalopathy: importance of total bilirubin, protein binding, and blood-brain barrier. *Pediatr. Res. 20*, 789−792.
(45) Kim, Y. R., Kim, H. N., Pak, M. E., Ahn, S. M., Hong, K. H., Shin, H. K., and Choi, B. T. (2015) Studies on the animal model of post-stroke depression and application of antipsychotic aripiprazole. *Behav. Brain Res. 287*, 294−303.

https://doi.org/10.1021/acschemneuro.1c00287
ACS Chem. Neurosci. 2021, 12, 2929−2939